Journal of Applied Physics

Non-volatile voltage control of in-plane and out-of-plane magnetization in polycrystalline Ni films on ferroelectric PMN–PT $(001)_{pc}$ substrates

Cite as: J. Appl. Phys. **129**, 154101 (2021); https://doi.org/10.1063/5.0040258
Submitted: 11 December 2020 • Accepted: 29 March 2021 • Published Online: 19 April 2021

M. Ghidini, F. Ye, N.-J. Steinke, et al.

Journal of Applied Physics ARTICLE scitation.org/journal/jap

Non-volatile voltage control of in-plane and out-of-plane magnetization in polycrystalline Ni films on ferroelectric PMN–PT $(001)_{pc}$ substrates

Cite as: J. Appl. Phys. **129**, 154101 (2021); doi: 10.1063/5.0040258
Submitted: 11 December 2020 · Accepted: 29 March 2021 ·
Published Online: 19 April 2021

M. Ghidini,[1,2,3,a)] F. Ye,[3] N.-J. Steinke,[4,b)] R. Mansell,[4,c)] C. H. W. Barnes,[4] and N. D. Mathur[3,a)]

AFFILIATIONS

[1]Department of Mathematics, Physics and Computer Science, University of Parma, Parma 43124, Italy
[2]Diamond Light Source, Chilton, Didcot, Oxfordshire OX11 0DE, United Kingdom
[3]Department of Materials Science, University of Cambridge, Cambridge CB3 0FS, United Kingdom
[4]Cavendish Laboratory, University of Cambridge, Cambridge CB3 0HE, United Kingdom

Note: This paper is part of the Special Topic on Domains and Domain Walls in Ferroic Materials.
[a)]**Authors to whom correspondence should be addressed:** massimo.ghidini@unipr.it and ndm12@cam.ac.uk
[b)]**Present address:** Institut Laue-Langevin, 71 Avenue des Martyrs, Grenoble 38042, France.
[c)]**Present address:** NanoSpin, Department of Applied Physics, Aalto University, Aalto, FI-00076, Finland.

ABSTRACT

We identify room-temperature converse magnetoelectric effects (CMEs) that are non-volatile by using a single-crystal substrate of PMN–PT $(001)_{pc}$ (pc denotes pseudocubic) to impart voltage-driven strain to a polycrystalline film of Ni. An appropriate magnetic-field history enhances the magnetoelectric coefficient to a near-record peak of $\sim 10^{-6}$ s m^{-1} and permits electrically driven magnetization reversal of substantial net magnetization. In zero magnetic field, electrically driven ferroelectric domain switching produces large changes of in-plane magnetization that are non-volatile. Microscopically, these changes are accompanied by the creation and destruction of magnetic stripe domains, implying the electrical control of perpendicular magnetic anisotropy. Moreover, the stripe direction can be rotated by a magnetic field or an electric field, the latter yielding the first example of electrically driven rotatable magnetic anisotropy. The observed CMEs are associated with repeatable ferroelectric domain switching that yields a memory effect. This memory effect is well known for PMN–PT $(110)_{pc}$ but not PMN–PT $(001)_{pc}$. Given that close control of the applied field is not required as for PMN–PT $(110)_{pc}$, this memory effect could lead the way to magnetoelectric memories based on PMN–PT $(001)_{pc}$ membranes that switch at low voltage.

I. INTRODUCTION

Magnetic memory devices can be more energy efficient if data are written using voltages rather than electric currents or their Oersted fields.[1–3] Consequently, there is now much interest in using voltages to modify magnetic properties and thus exploiting converse magnetoelectric effects (CMEs).[4–9] Single-phase multiferroic materials tend to show voltage-driven magnetic changes that are largest at low temperatures but nevertheless small.[10–12] Applications are, therefore, more likely to be achieved by exploiting the large CMEs that arise at room temperature in multiferroic heterostructures, where a ferromagnetic film is addressed via strain,[13–23] charge,[24–28] or exchange bias[29–31] from a juxtaposed ferroelectric material. Here, we focus on strain-mediated CMEs, where inverse magnetostriction in a polycrystalline ferromagnetic film is triggered by the electroactive response (piezoelectricity or domain switching) of ferroelectric substrates, most typically single crystals of $BaTiO_3$ (BTO) or $(1-x)Pb(Mg_{1/3}Nb_{2/3})O_3$–$xPbTiO_3$ (PMN–PT) with $x \sim 0.3$.

Ferromagnetic films on PMN–PT substrates represent an exciting playground for strain-mediated CMEs.[13–23] These CMEs are non-volatile if PMN–PT adopts the $(110)_{pc}$ orientation and if applied fields closely match the coercive field.[16–21] By contrast, the $(001)_{pc}$ orientation of PMN–PT typically results in volatile

CMEs,[13] but it can also result in non-volatile CMEs with no need for close control of applied field magnitude,[22] as we will see here by studying the in-plane (IP) and out-of-plane (OOP) magnetization of a 100-nm-thick film of Ni on PMN–PT $(001)_{pc}$ ($x \sim 0.28$).

Here, as usual, we identify magnetic changes in the film when a voltage that is applied between this film and a back electrode on the substrate causes the substrate and thus the film to deform. We first present macroscopic non-volatile CMEs, where a negative electric field induces uniaxial IP magnetic anisotropy via 109° ferroelectric domain switching in specific directions and where a positive electric field destroys this anisotropy. We also demonstrate electrically induced magnetization reversal in the presence of a magnetic field. Our previous work with surface-sensitive measurements demonstrates complete strain transfer from thick ferroelectric substrates to much thinner 100 nm-thick films of Ni as expected,[32] and we will assume that CMEs measured in our polycrystalline film reflect the strain-field behavior of our PMN–PT $(001)_{pc}$ substrate, as seen elsewhere.[15,33]

Microscopically, our virgin Ni film displays magnetic stripe domains. These stripe domains arise in our polycrystalline film because a small uniaxial OOP stress anisotropy competes with dominant IP shape anisotropy to cant the local magnetization slightly up and down in alternating stripe domains.[34,35] Given that Ni shows negative magnetostriction, the OOP anisotropy is understood to originate from an isotropic planar growth stress that is tensile.[32,36,37]

We present microscopic CMEs in which electrically induced ferroelectric domain switching overcomes the growth stress in the film[32] to annihilate stripe domains. The stripes reappear after the ferroelectric domains switch back, and the process is repeatable over at least 10 cycles. The stripe domains can be rotated with an IP magnetic field, demonstrating that our as-grown films possess rotatable magnetic anisotropy (RMA, which led to the discovery of stripe domains).[37–39] The stripe domains in our films can also be rotated by electrically switching the ferroelectric domains. This non-volatile rotation is a consequence of uniaxial film stress arising from 109° ferroelectric domain switching, and it represents the first demonstration of electrically driven RMA.

II. METHODS

A 100 nm-thick polycrystalline film of Ni was grown at ~0.3 nm/min on a $5 \times 5 \times 0.3$ mm^3 substrate of unpoled PMN–PT $(001)_{pc}$ using room-temperature e-beam-assisted evaporation with a base pressure of 1.5×10^{-10} mbar. Using the same growth technique, the Ni film was capped with 4 nm of Cu to prevent oxidation. From our previous work on similar films,[32] the Ni grain size is over 100 nm, and there is no evidence for preferred orientations. IP crystallographic orientation was inferred from knowledge of PMN–PT domain geometry. Magnetization measurements were performed using a Princeton Measurements Corporation vibrating sample magnetometer (VSM), with electrical access to the sample.[40] All bipolar sweeps of the magnetic field were performed in ±0.4 MA m^{-1} and are presented in a smaller field range. Magnetic force microscopy (MFM) measurements were performed using a Digital Instruments Dimension 3100, at lift heights of 40–60 nm, using low-moment ASYMFMLM Asylum Research tips that were coated with 15 nm of CoCr. The cantilever stiffness was 2 N m^{-1}. These tips and the Ni film were both grounded to minimize noise and keep them at the same potential. All MFM image analysis was performed using WSxM software.[41] During VSM measurements, the Ni film was also grounded. Positive and negative voltages were applied to a 200 nm-thick back electrode of Pt, and the sign of the applied voltage identifies the sign of the resulting electric field in the PMN–PT substrate.

III. RESULTS

A. Macroscopic magnetoelectric effects

Topographical scans that we acquired during our MFM measurements revealed the roughness of the Ni film to be 1 nm. Major IP magnetic hysteresis loops measured (plotted) out to ±0.4 MA m^{-1} (±0.08 MA m^{-1}) at increasing values of the positive electric field [Fig. 1(a)] reveal a CME in which the electric field linearly increases remanent magnetization M_r and linearly decreases the coercive field H_c, and the increase and decrease both measure 30% at our maximum field of $E = +1.33$ MV m^{-1}. By contrast, the corresponding OOP measurements [Fig. 1(b)] show that the positive electric field linearly increases the saturation field. These IP and OOP measurements self-consistently imply an electrically driven increase (suppression) of a relatively large IP (relatively small OOP) anisotropy, and subsequent observations confirmed that these CMEs are volatile. We, therefore, identify these high-positive-field CMEs with piezostrains that are compressive along all IP directions on average [see Fig. 4(b), later]. If we instead use the electric field to switch ferroelectric domains, then we will see that Ni/PMN–PT represents a rich playground in which to investigate CMEs.

The state of this playground depends on the magnetic history of the sample. To show this, we will investigate CMEs after starting from three different magnetic states that we identify via the IP hysteresis measurement for $E = 0$ [see Fig. 2(a), which represents a zoom of Fig. 1(a) out to the smaller field of ±0.04 MA m^{-1}]. State S1 is a magnetically remanent state after saturating with a large positive field of $H = +0.4$ MA m^{-1}. State S2 is reached after reducing a large positive field of $H = +0.4$ MA m^{-1} down to $H = +0.08$ MA m^{-1}. State S3 is reached after increasing a large negative field of $H = -0.4$ MA m^{-1} to reach a positive field of $H = +0.08$ MA m^{-1}. After reaching each of these three magnetic states, we performed bipolar sweeps in which the electric field was first negative and then positive, resulting in CMEs that are large and non-volatile [Figs. 2(b), 2(d), and 2(f)]. This result contrasts the small and volatile CMEs that we obtained with unipolar sweeps of a positive electric field (Fig. 1). For state S1, the negative voltage sweep from $E = 0$ to $E = -0.4$ MV m^{-1} produces a 62% increase in magnetization, most of which is non-volatile given that this increase is reduced to 53% after removing the electric field (i.e., the magnetizations of electrically remanent states A1 and B1 differ by 53%). For state S2, the negative voltage sweep from $E = 0$ to $E = -0.24$ MV m^{-1} produces a 36% increase in magnetization, most of which is also non-volatile given that this increase is reduced to 30% after removing the electric field (i.e., the magnetizations of electrically remanent states A2 and B2 differ by 30%).

For state S3, the negative voltage sweep from $E = 0$ to $E = -0.24$ MV m^{-1} produces a giant 200% increase in magnetization,

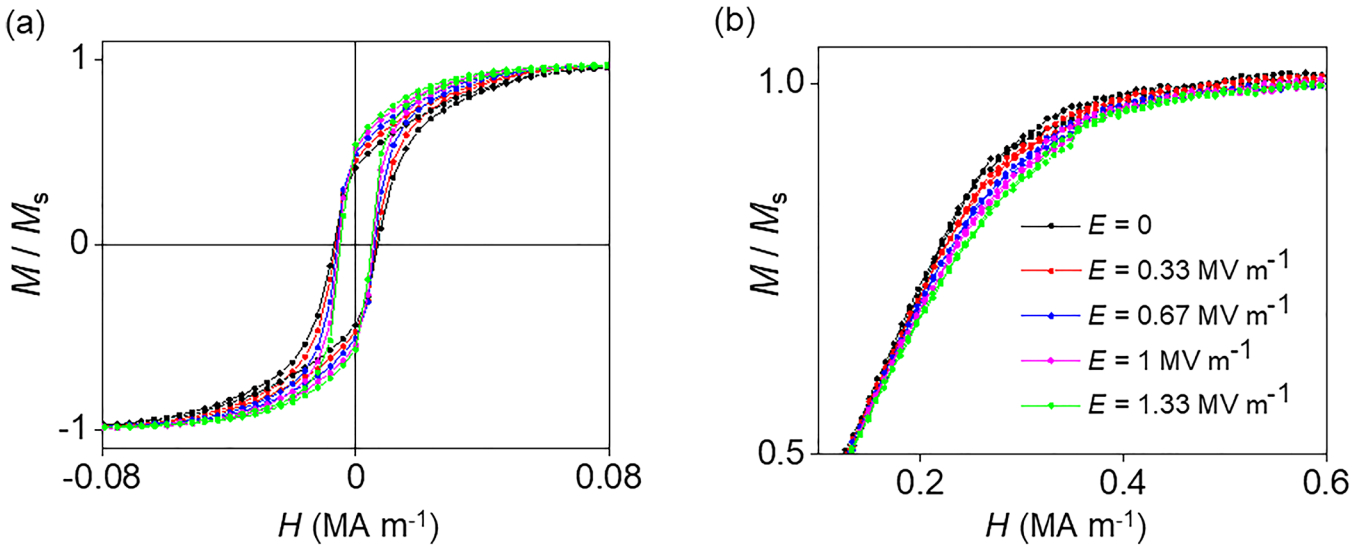

FIG. 1. Volatile *ME* effects with positive electric fields. (a) IP and (b) OOP reduced magnetization M/M_s vs collinear magnetic field H for selected values of electric field E. Data in (a) were measured out to ±0.4 MA m^{-1}. Figure 4(b) shows that the increased remanence in (a) arises along all IP directions when applying $E = +0.33$ MV m^{-1}. Saturation magnetization $M_s = 185$ kA m^{-1}.

most of which is yet again non-volatile given that this increase is reduced to 185% after removing the electric field (i.e., the magnetizations of electrically remanent states A3 and B3 differ by 185%). After subsequently sweeping the field to $E = +0.16$ MV m^{-1} and then back to $E = 0$, repeating the negative field sweep produces a smaller 44% increase in magnetization, most of which is non-volatile given that this increase is reduced to 36% after removing the electric field (i.e., the magnetizations of electrically remanent states C3 and B3 differ by 36%). However, the giant change 200% can be repeated by repeating the magnetic preparation of state S3 [Fig. 2(a)] with $E = 0$.

Figures 2(c), 2(e), and 2(g) show that the CME coupling coefficients $\alpha = \mu_0 dM/dE$ associated with states S1–S3 present sharp minima, with peak magnitudes ranging from 3×10^{-7} s m^{-1} [Fig. 2(c)] to 4.9×10^{-7} s m^{-1} [Fig. 2(e)] to $\sim 10^{-6}$ s m^{-1} [Fig. 2(g)]. These values exceed the value of 2.3×10^{-7} s m^{-1} for epitaxial films of $La_{0.67}Sr_{0.33}MnO_3$ on $BaTiO_3$ $(001)_{pc}$[40] and lie close to the record value of 7.4×10^{-6} s m^{-1}, which was achieved for polycrystalline films of $Co_{40}Fe_{40}B_{20}$ on PMN–PT $(110)_{pc}$.[42]

Figure 3(a) shows two major IP magnetic hysteresis loops that start from the electrically and magnetically remanent states A1 and B1′, where B1′ was prepared from A1 by applying and removing a negative field of $E = -0.33$ MV m^{-1} (above we used $E = -0.4$ MV m^{-1} to convert A1 to B1, but here we use a field of smaller magnitude to reduce the risk of fatigue and failure, such that the 30% discrepancy in the magnetization of A1 and B1′ is smaller than the 53% discrepancy in the magnetization of A1 and B1). Alternating voltage pulses of opposite polarity [Fig. 3(b)] repeatably interconvert two stable states whose magnetizations match well with the magnetizations of states A1 and B1′ [Fig. 3(c)]. Figure 4(a) shows major IP magnetic hysteresis loops for these two electrically interconverted states, as well as the initial state with $E = 0$. The corresponding polar plots of loop squareness [Fig. 4(b)] show that the negative electric field induces a uniaxial magnetic anisotropy and enhances magnetic remanence, and that the positive electric field restores the isotropic magnetic state and small magnetic remanence [Figs. 4(a) and 4(b)]. Note that the effect of the negative electric field here is non-volatile, and although we did not show this using polar plots, it follows from Fig. 2(b).

The electrical control of magnetic coercivity observed in Fig. 3(a) presages an electrically driven magnetization switching, and this switching is large and irreversible (Fig. 5). After increasing a large negative field to a small positive value of $H_1 = 0.0048$ MA m^{-1} or $H_2 = 0.0064$ MA m^{-1}, the subsequent application of $E = -0.33$ MV m^{-1} reverses the direction of net magnetization, and the resulting states lie on the lower branch of the orange hysteresis loop that was obtained after setting state B1′ by applying and removing the same field of $E = -0.33$ MV m^{-1}. If instead one increases the large negative field to slightly larger positive fields of $H_3 = 0.0080$ MA m^{-1} or $H_4 = 0.0096$ MA m^{-1}, such that the net magnetization switches from negative to positive, then the subsequent application of $E = -0.33$ MV m^{-1} increases the magnetization to yield a state that lies on the upper branch of the purple hysteresis loop. This is surprising given that the purple hysteresis loop was obtained after setting state A1 by applying and removing $E = +0.33$ MV m^{-1} rather than $E = -0.33$ MV m^{-1}. However, the common feature is that the electric field increases the magnetization by the smallest possible amount that brings the system to a branch of the orange or the purple hysteresis loop, implying a rich complexity in which metastable states populate a complex and hysteretic energy landscape on (H,E) axes.

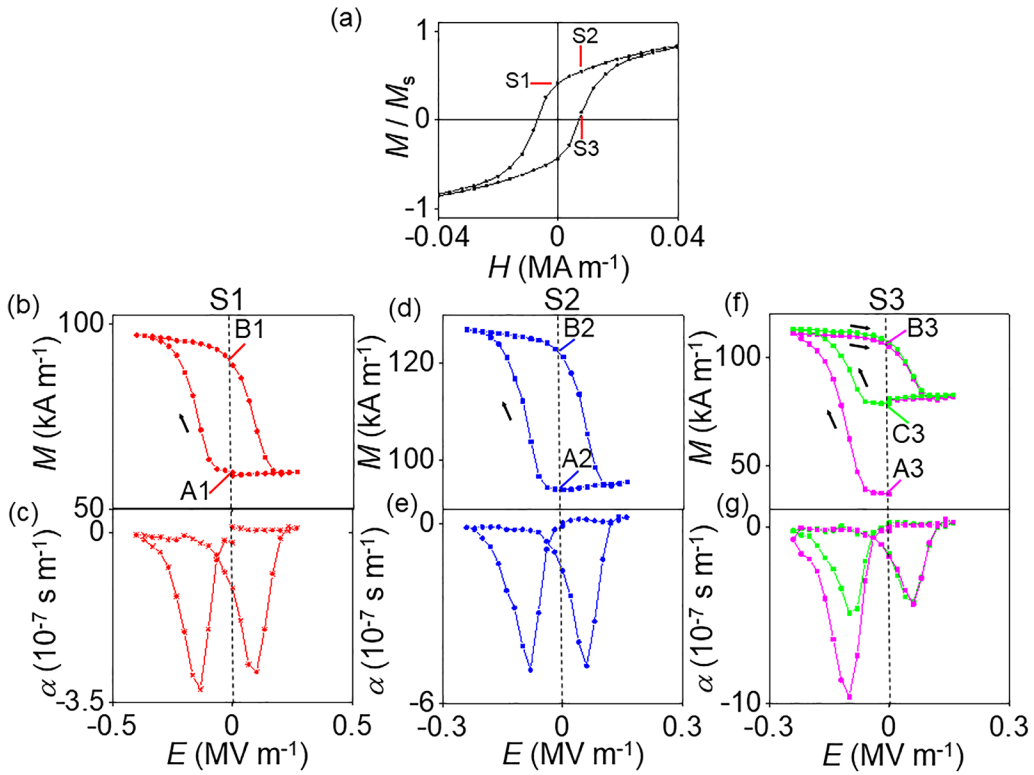

FIG. 2. Giant and non-volatile *ME* effects with electric fields that are initially negative, and the role of magnetic-field history. (a) The central part of the IP hysteresis loop at $E = 0$ [Fig. 1(a)] is repeated here to define state S1 at $H = 0$ and states S2 and S3 at $H = +0.08$ MA m^{-1}. (b)–(g) For starting states S1–S3, we show $M(E)$ and the corresponding *ME* coupling coefficient $\alpha = \mu_0 dM/dE$. The states A1, A2, and A3 were obtained at $E = 0$ following the application of the positive electric field in Fig. 1. Subsequent electric field cycling led to states B1, B2, B3, and C3 at $E = 0$.

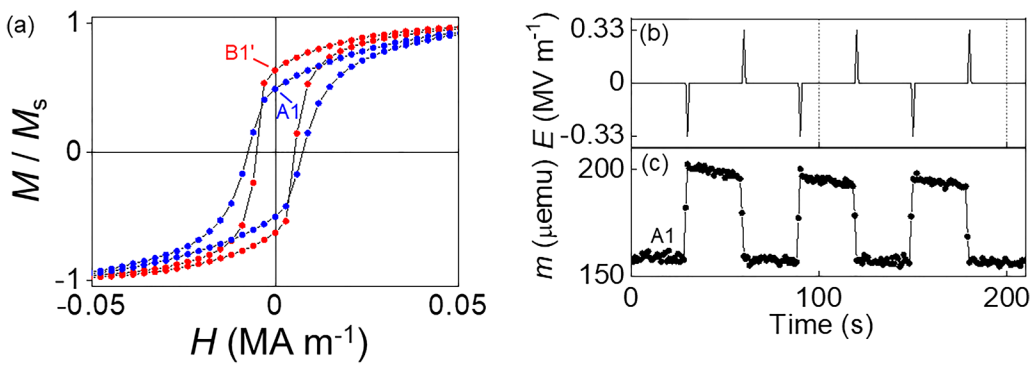

FIG. 3. Repeatable non-volatile *ME* switching with no magnetic field. (a) IP reduced magnetization M/M_s vs collinear magnetic field H measured out to ±0.4 MA m^{-1} after starting at $H = 0$ in states A1 and B1′. The preparation of A1 is shown in Fig. 2(b). State B1′ was obtained by preparing state A1 and then applying and removing a negative field of $E = -0.33$ MV m^{-1} (cf. state B1 created from A1 with $E = -0.4$ MV m^{-1}). (b) and (c) Starting in state A1, (b) opposite-sign pulses of electric field E produce (c) a non-volatile and repeatable switching of the magnetic moment m that may be considered to represent switching between states corresponding to A1 and B1′.

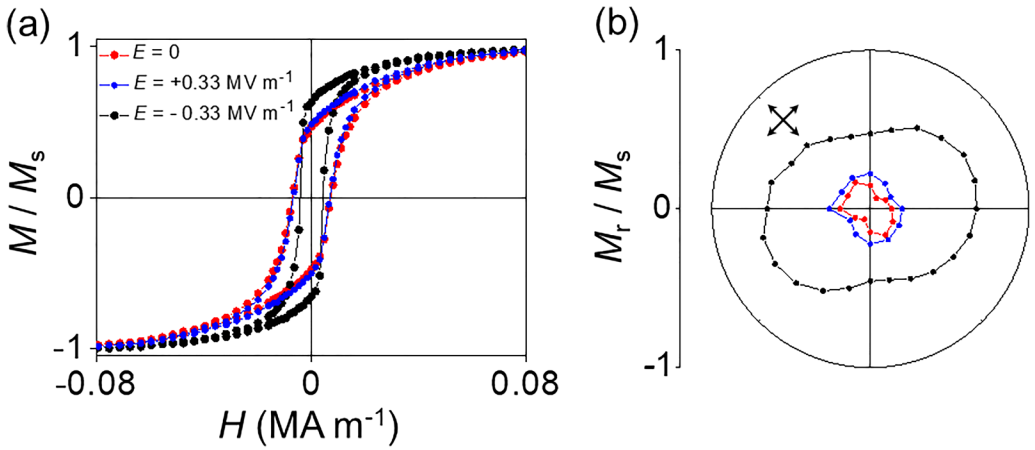

FIG. 4. Electrically induced uniaxial anisotropy. (a) IP component of reduced magnetization M/M_s vs collinear magnetic field H measured out to ±0.4 MA m^{-1} for the <110>$_{pc}$ direction, with $E = 0$, then $E = +0.33$ MV m^{-1}, and then $E = -0.33$ MV m^{-1}. (b) Polar plots of loop squareness M_r/M_s derived from hysteresis loops such as those shown in (a), where M_r denotes remanent magnetization. Crossed arrows denote <110>$_{pc}$ directions. Red and blue data were mirrored to construct the lower half of the polar plot.

B. Microscopic magnetoelectric effects

The electrical field sweep in Fig. 2(b) involves the creation and annihilation of magnetic stripe domains (Fig. 6), whose presence at $E = 0$ can be considered ubiquitous after close inspection of the MFM images for states A1 and G. The stripe domains represent a manifestation of the small and electrically controlled uniaxial OOP anisotropy that was evidenced in our macroscopic OOP measurements using a positive electric field [Fig. 1(b)]. The initial A1 state at $E = 0$ presents a stripe domain pattern with stripe width $W = 193 \pm 15$ nm, such that the OOP anisotropy constant is found to be $K_z \sim 19$ kJ m^{-3} from the following expression:[36]

$$K_z = \frac{\pi^2}{D^2}\left(\frac{D^2}{W^2} + 1\right)^2 A,$$

where film thickness $D = 100$ nm and exchange stiffness $A = 0.82 \times 10^{-11}$ J m^{-1}.[43] The OOP anisotropy arises due to a growth stress of $-\frac{2}{3}K_z\lambda_s^{-1} = +0.4$ GPa,[32] which is similar to growth stress in other polycrystalline metallic films,[44] and similar to the value for similar Ni films that were grown on $BaTiO_3$ in the same deposition system[32] (the saturation magnetostriction for room-temperature Ni is $\lambda_s = -32.9 \times 10^{-6}$). Stripe domains undergo progressive and ultimately complete elimination due to negative electric fields of increasing magnitude (A1 → C → D → E, Fig. 6), partial reset on returning to $E = 0$ (B1, Fig. 6), and complete reset by a positive field (F, Fig. 6) such that they persist after this field has been removed (G, Fig. 6). The initial application of a negative electric field, thus, yields non-volatile changes of OOP anisotropy at seemingly all locations in our MFM field of view.

Let us now consider the effect of magnetic and then electric fields on stripe orientation. Figure 7 shows that a sufficiently large magnetic field produces a non-volatile alignment of the stripes with respect to the field direction. This represents an example of magnetically induced RMA, which is a well-known phenomenon.[37–39] By contrast, Fig. 8 shows that a sufficiently large electric field produces a non-volatile alignment of the stripes with respect to the <110>$_{pc}$ direction (Fig. 4). This represents an example of electrically induced RMA, which is novel.

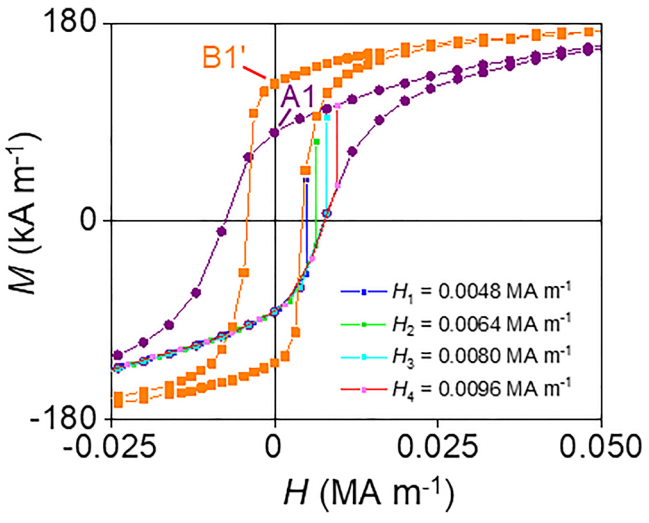

FIG. 5. Electrically driven magnetization reversal at constant magnetic field. We show part of the major IP magnetic hysteresis loops that were measured out to ±0.4 MA m^{-1} after starting in states A1 (purple) and B1′ (orange) at $H = E = 0$. After having started in state A1, increasing H from the largest negative field ($H = -0.4$ MA m^{-1}) to a positive field (specified in the legend) and then applying $E = -0.33$ MV m^{-1} results in a jump of M that approximately reaches a branch on one of the as-shown magnetic hysteresis loops.

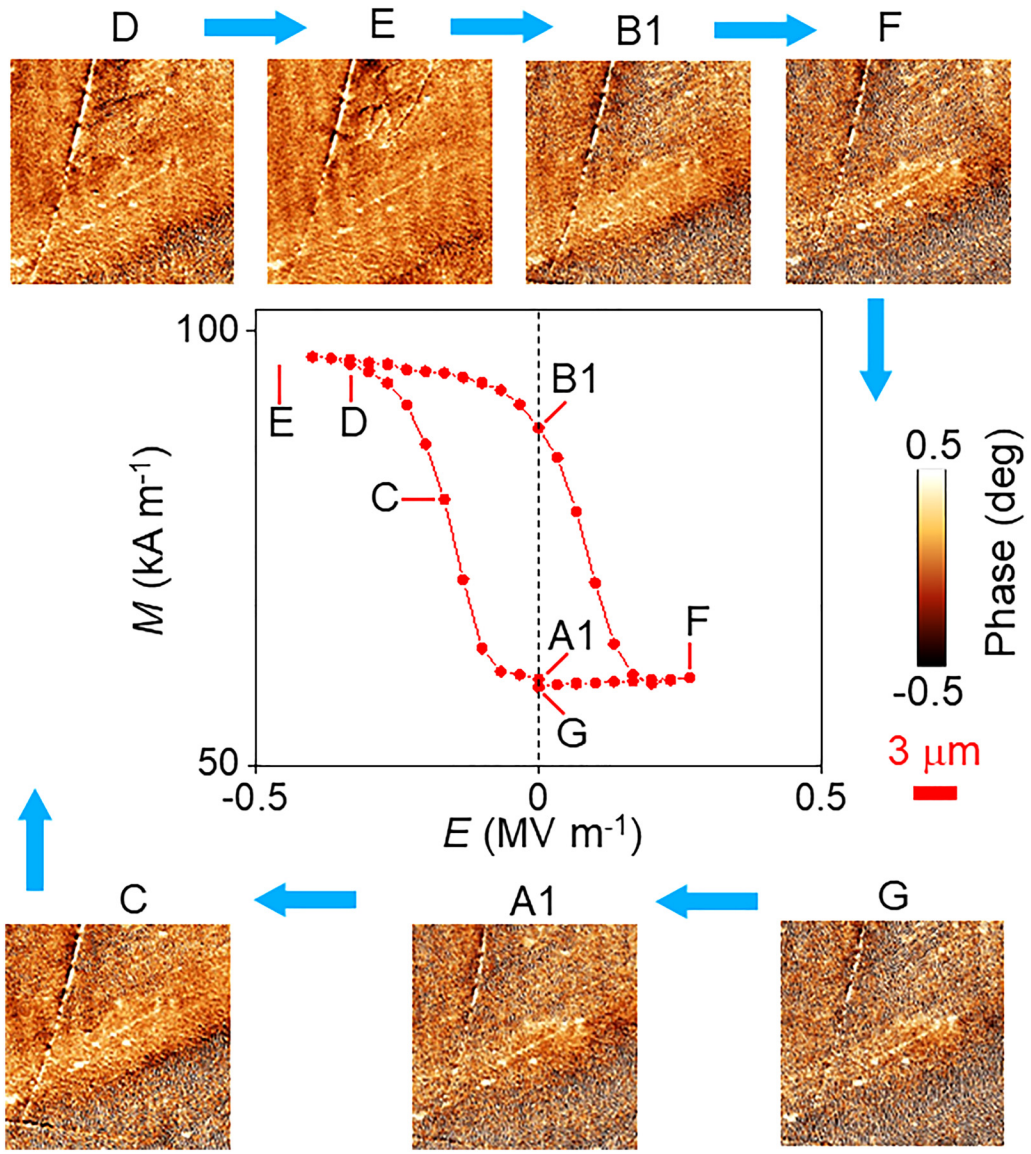

FIG. 6. MFM images with an applied electric field. The central plot showing $M(E)$ from Fig. 2(b) is labelled to identify the seven corresponding MFM images. These images were obtained in the order shown by blue arrows, starting with the image for state A1. The image for state E was obtained beyond the largest negative field used when measuring $M(E)$.

IV. DISCUSSION

Let us now understand the field asymmetry in our CMEs during bipolar cycles [Figs. 2(b), 2(d), and 2(f)], which display non-volatile and repeatable switching [Figs. 3(b) and 3(c)]. Negative electric fields result in a uniaxial IP magnetic anisotropy [black data, Fig. 4(b)] and a concomitantly high moment along the measurement direction [Figs. 3(b) and 3(c)], while positive electric fields recover the IP magnetic isotropy [blue data, Fig. 4(b)] and a concomitantly low moment along the measurement direction [Figs. 3(b) and 3(c)]. At negative (positive) electric fields, the uniaxial IP magnetic anisotropy is created (destroyed) by IP compression (tension) along the $<110>_{pc}$ direction, which is accompanied by a relatively small tensile (compressive) strain along the perpendicular IP direction, implying that bipolar ferroelectric domain switching is dominated by 109° switching in specific directions.

Overall, we, therefore, find that a sufficiently large positive electric field results each time in a ferroelectric domain configuration that confers IP isotropy on the as-grown film and that a

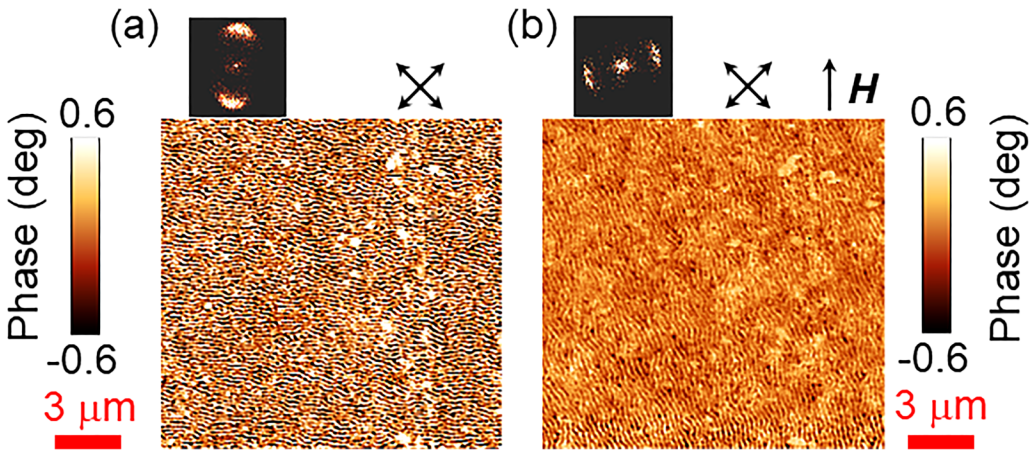

FIG. 7. Magnetically induced rotation of stripe domains. MFM images of a 15 × 15 μm^2 region of the sample (a) before and (b) after applying a field of $H = 0.1$ MA m^{-1} along the IP direction marked by the single-headed arrow. Crossed arrows denote $<110>_{pc}$ directions. The rotation of the stripes can be appreciated by viewing the images at a glancing angle or from the 5.5 × 5.5 μm^{-2} fast Fourier transforms that appear above the images.

sufficiently large negative electric field results each time in a ferroelectric domain configuration that confers uniaxial IP anisotropy on the film. This repeatable asymmetry is attributed to ordered dipole defects that arise from oxygen vacancies and impart an internal bias field,[45–47] and the phenomenon was recently exploited to control PMN–PT $(110)_{pc}$ and the resulting CMEs.[48] In other words, PMN–PT $(001)_{pc}$ here (and in Ref. 22), and PMN–PT $(110)_{pc}$ in Ref. 48 (and in Ref. 42) display a memory effect. The repeatable asymmetry underpins electrically driven switching between the different branches of different magnetic hysteresis loops at finite magnetic fields (Fig. 5), resulting in large CMEs. The concomitant creation and destruction of stripe domains (Fig. 6) demonstrate that the Ni//PMN–PT $(001)_{pc}$ system offers control of both IP and OOP magnetic phenomena.

Ferromagnetic films on PMN–PT $(001)_{pc}$ substrates sometimes display asymmetric CMEs of the type we find here [loop-like $M(E)$],[22] but it is more common for them to display symmetric CMEs [butterfly-like $M(E)$][13] when most ferroelectric domains switch by 71° (or 180°), such that electrically induced changes of IP strain are volatile. Likewise, the ferromagnetic films on PMN–PT $(110)_{pc}$ substrates can present loop-like[42,47] or butterfly-like $M(E)$ behavior,[23] while butterfly-like behavior can in effect be converted to loop-like behavior by making the loops minor.[17] In future, it would be interesting to exert deterministic control over ferroelectric

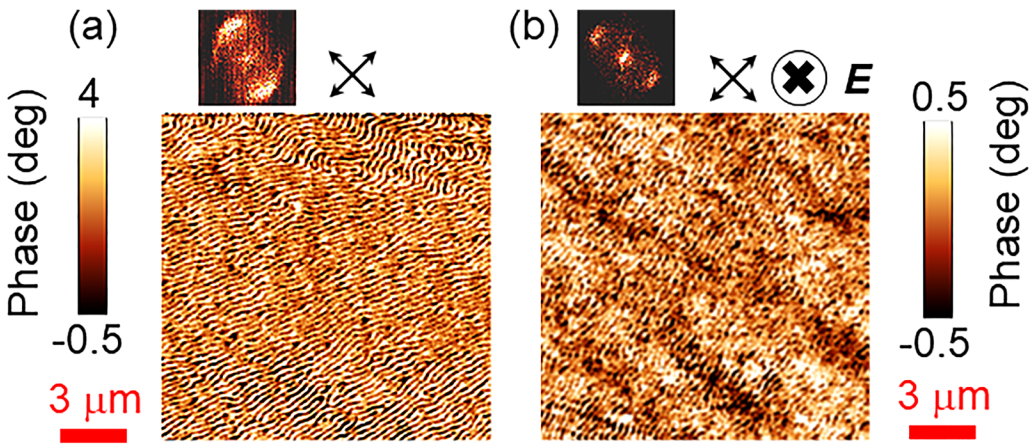

FIG. 8. Electrically induced rotation of stripe domains. MFM images for a 15 × 15 μm^2 region of the sample (a) before and (b) after applying a field of $E = -0.33$ MV m^{-1} along the OOP direction marked by the tail-end view of what is a single-headed arrow. Crossed arrows denote $<110>_{pc}$ directions. The rotation of the stripes can be appreciated by viewing the images at a glancing angle or from the 5.5 × 5.5 μm^{-2} fast Fourier transforms that appear above the images.

switching pathways in PMN–PT, as this would represent a key step in the development of magnetoelectric memory cells. These cells could be based on PMN–PT membranes, which avoid the constraint of a fixed substrate and switch at low voltage.[49] It would also be interesting to perform more detailed imaging studies, e.g., using photoemission electron microscopy (PEEM) with magnetic contrast from x-ray magnetic circular dichroism (XMCD),[50] in order to see how the shear associated with ferroelectric domain switching in PMN–PT[23] influences the details of local stripe orientation.

ACKNOWLEDGMENTS

This work was funded by Isaac Newton Trust Grant [Nos. 10.26(u) and 11.35(u)] and UK EPSRC Grant No. EP/G031509/1.

DATA AVAILABILITY

The data that support the findings of this study are available from the corresponding authors upon reasonable request.

REFERENCES

[1]M. Bibes and A. Barthélémy, Nat. Mat. **7**, 425 (2008).
[2]J.-M. Hu, Z. Li, L. Q. Chen, and C. W. Nan, Nat. Comm. **2**, 553 (2011).
[3]J.-M. Hu and C. W. Nan, APL Mater. **7**, 080905 (2019).
[4]N. A. Spaldin and R. Ramesh, Nat. Mater. **18**, 203 (2019).
[5]S.-W. Cheong and M. Mostvoy, Nat. Mat. **6**, 13 (2007).
[6]C.-W. Nan, M. I. Bichurin, S. Dong, D. Viehland, and G. Srinivasan, J. Appl. Phys. **103**, 031101 (2008).
[7]H. Ohno, D. Chiba, F. Matsukura, T. Omiya, E. Abe, T. Dietl, Y. Ohno, and K. Ohtani, Nature **408**, 944 (2000).
[8]D. Chiba, M. Yamanouchi, F. Matsukura, and H. Ohno, Science **301**, 943 (2003).
[9]D. Chiba, M. Sawicki, Y. Nishitani, Y. Nakatani, F. Matsukura, and H. Ohno, Nature **455**, 515 (2008).
[10]R. Tang, H. Zhou, W. You, and H. Yang, Appl. Phys. Lett. **109**, 082903 (2016).
[11]Y. Kitagawa, Y. Hiraoka, T. Honda, T. Ishikura, H. Nakamura, and T. Kimura, Nat. Mater. **9**, 797 (2010).
[12]J. F. Scott, NPG Asia Mater. **5**, e72 (2013).
[13]C. Thiele, K. Dörr, O. Bilani, J. Rödel, and L. Schultz, Phys. Rev. B **75**, 054408 (2007).
[14]S. Sahoo, S. Polisetty, C. G. Duan, S. S. Jaswal, E. Y. Tsymbal, and C. Binek, Phys. Rev. B **76**, 092108 (2007).
[15]S. Geprägs, A. Brandlmaier, M. Opel, R. Gross, and S. T. B. Goennenwein, Appl. Phys. Lett. **96**, 142509 (2010).
[16]T. Wu, A. Bur, P. Zhao, K. P. Mohanchandra, K. Wong, K. L. Wang, C. S. Lynch, and G. P. Carman, Appl. Phys. Lett. **98**, 012504 (2011).
[17]T. Wu, A. Bur, K. Wong, P. Zhao, C. S. Lynch, P. Khalili Amiri, K. L. Wang, and G. P. Carman, Appl. Phys. Lett. **98**, 262504 (2011).
[18]T. H. E. Lahtinen, K. J. A. Franke, and S. van Dijken, Sci. Rep. **2**, 258 (2012).
[19]R. O. Cherifi, V. Ivanovskaya, L. C. Phillips, A. Zobelli, I. C. Infante, E. Jacquet, V. Garcia, S. Fusil, P. R. Briddon, N. Guiblin, A. Mougin, A. A. Ünal, F. Kronast, S. Valencia, B. Dkhil, A. Barthélémy, and M. Bibes, Nat. Mater. **13**, 345 (2014).
[20]M. Liu, B. M. Howe, L. Grazulis, K. Mahalingam, T. Nan, N. X. Sun, and G. J. Brown, Adv. Mater. **25**, 4886 (2013).
[21]T. Wu, P. Zhao, M. Bao, A. Bur, J. L. Hockel, K. Wong, K. P. Mohanchandra, C. S. Lynch, and G. P. Carman, J. Appl. Phys. **109**, 124101 (2011).
[22]S. Zhang, Y. G. Zhao, P. S. Li, J. J. Yang, S. Rizwan, J. X. Zhang, J. Seidel, T. L. Qu, Y. J. Yang, Z. L. Luo, Q. He, T. Zou, Q. P. Chen, J. W. Wang, L. F. Yang, Y. Sun, Y. Z. Wu, X. Xiao, X. F. Jin, J. Huang, C. Gao, X. F. Han, and R. Ramesh, Phys. Rev. Lett. **108**, 137203 (2012).
[23]M. Ghidini, R. Mansell, F. Maccherozzi, X. Moya, L. C. Phillips, W. Yan, D. Pesquera, C. H. W. Barnes, R. P. Cowburn, J.-M. Hu, S. S. Dhesi, and N. D. Mathur, Nat. Mater. **18**, 840 (2019).
[24]T. Maruyama, Y. Shiota, T. Nozaki, K. Ohta, N. Toda, M. Mizuguchi, A. A. Tulapurkar, T. Shinjo, M. Shiraishi, S. Mizukami, Y. Ando, and Y. Suzuki, Nat. Nano. **4**, 158 (2009).
[25]M. Endo, S. Kanai, S. Ikeda, F. Matsukura, and H. Ohno, Appl. Phys. Lett. **96**, 212503 (2010).
[26]M. Weisheit, S. Fähler, A. Marty, Y. Souche, C. Poinsignon, and D. Givord, Science **315**, 349 (2007).
[27]L. Shu, Z. Li, J. Ma, Y. Gao, L. Gu, Y. Shen, Y. Lin, and C. W. Nan, Appl. Phys. Lett. **100**, 022405 (2012).
[28]J.-M. Hu, C. W. Nan, and L.-Q. Chen, Phys. Rev. B **83**, 134408 (2011).
[29]V. Skumryev, V. Laukhin, I. Fina, X. Martí, F. Sánchez, M. Gospodinov, and J. Fontcuberta, Phys. Rev. Lett. **106**, 057206 (2011).
[30]J. T. Heron, J. L. Bosse, Q. He, Y. Gao, M. Trassin, L. Ye, J. D. Clarkson, C. Wang, J. Liu, S. Salahuddin, D. C. Ralph, D. G. Schlom, J. Íñiguez, B. D. Huey, and R. Ramesh, Nature **516**, 370 (2014).
[31]J. T. Heron, D. G. Schlom, and R. Ramesh, Appl. Phys. Rev. **1**, 021303 (2014).
[32]M. Ghidini, F. Maccherozzi, X. Moya, L. C. Phillips, W. Yan, J. Soussi, N. Métallier, M. E. Vickers, N.-J. Steinke, R. Mansell, C. H. W. Barnes, S. S. Dhesi, and N. D. Mathur, Adv. Mater. **27**, 1460 (2015).
[33]C. Israel, S. Kar-Narayan, and N. D. Mathur, Appl. Phys. Lett. **93**, 173501 (2008).
[34]N. Saito, H. Fujiwara, and Y. Sugita, J. Phys. Soc. Jpn. **19**, 1116 (1964).
[35]G. Asti, M. Ghidini, M. Mulazzi, R. Pellicelli, M. Solzi, K. Chesnel, and A. Marty, Phys. Rev. B **76**, 094414 (2007).
[36]A. Hubert and R. Schäfer, *Magnetic Domains* (Springer-Verlag, Berlin, 1998).
[37]S. Fin, R. Tomasello, D. Bisero, M. Marangolo, M. Sacchi, H. Popescu, M. Eddrief, C. Hepburn, G. Finocchio, M. Carpentieri, A. Rettori, M. G. Pini, and S. Tacchi, Phys. Rev. B **92**, 224411 (2015).
[38]R. J. Prosen, J. O. Holmen, and B. E. Gran, J. Appl. Phys. **32**, S91 (1961).
[39]S. S. Lehrer, J. Appl. Phys. **34**, 1207 (1963).
[40]W. Eerenstein, M. Wiora, J. L. Prieto, J. F. Scott, and N. D. Mathur, Nat. Mat. **6**, 348 (2007).
[41]I. Horcas, R. Fernandez, J. M. Gomez-Rodriguez, J. Colchero, J. Gomez-Herrero, and A. M. Baro, Rev. Sci. Instrum. **78**, 013705 (2007).
[42]J. Wang, D. Pesquera, R. Mansell, S. van Dijken, R. P. Cowburn, M. Ghidini, and N. D. Mathur, Appl. Phys. Lett. **114**, 092401 (2019).
[43]A. Michels, J. Weissmüller, A. Wiedenmann, and J. G. Barker, J. Appl. Phys. **87**, 5953 (2000).
[44]L. B. Freund and S. Suresh, *Thin Film Materials: Stress, Defect Formation and Surface Evolution* (Cambridge University Press, Cambridge, 2003), pp. 63–70 and 597.
[45]K. Carl and K. H. Hardtl, Ferroelectrics **17**, 473 (1977).
[46]U. Robels and G. Arlt, J. Appl. Phys. **73**, 3454 (1993).
[47]C. Yang, E. Sun, B. Yang, and W. Cao, J. Phys. D: Appl. Phys. **51**, 415303 (2018).
[48]W. Du, M. Liu, H. Su, H. Zhang, B. Liu, H. Meng, G. Xu, R. Peng, and X. Tang, Appl. Phys. Lett. **117**, 222401 (2020).
[49]H. S. Kum, H. Lee, S. Kim, S. Lindemann, W. Kong, K. Qiao, P. Chen, J. Irwin, J. H. Lee, S. Xie, S. Subramanian, J. Shim, S.-H. Bae, C. Choi, L. Ranno, S. Seo, S. Lee, J. Bauer, H. Li, K. Lee, J. A. Robinson, C. A. Ross, D. G. Schlom, M. S. Rzchowski, C.-B. Eom, and J. Kim, Nature **578**, 75 (2020).
[50]M. Ghidini, S. S. Dhesi, and N. D. Mathur, J. Magn. Magn. Mater. **520**, 167016 (2021).